JACS
JOURNAL OF THE AMERICAN CHEMICAL SOCIETY

Article

pubs.acs.org/JACS

Solution Structures of Hauser Base $^{i}Pr_2NMgCl$ and *Turbo*-Hauser Base $^{i}Pr_2NMgCl{\cdot}LiCl$ in THF and the Influence of LiCl on the Schlenk-Equilibrium

Roman Neufeld,[†] Thorsten L. Teuteberg,[‡] Regine Herbst-Irmer,[†] Ricardo A. Mata,[‡] and Dietmar Stalke*[,†]

[†]Institut für Anorganische Chemie, Georg-August-Universität, Tammannstrasse 4, D-37077 Göttingen, Germany

[‡]Institut für Physikalische Chemie, Georg-August-Universität, Tammannstrasse 6, D-37077 Göttingen, Germany

Supporting Information

ABSTRACT: Grignard reagents that are at the simplest level described as "RMgX" (where R is an organic substituent and X a halide) are one of the most widely utilized classes of synthetic reagents. Lately, especially Grignard reagents with amido ligands of the type R_1R_2NMgX, so-called Hauser bases, and their *Turbo* analogue $R_1R_2NMgX{\cdot}LiCl$ play an outranging role in modern synthetic chemistry. However, because of their complex solution behavior, where Schlenk-type equilibria are involved, very little is known about their structure in solution. Especially the impact of LiCl on the Schlenk-equilibrium was still obscured by complexity and limited analytical access. Herein, we present unprecedented insights into the solution structure of the Hauser base $^{i}Pr_2NMgCl$ **1** and the *Turbo*-Hauser base $^{i}Pr_2NMgCl{\cdot}LiCl$ **2** at various temperatures in THF-d_8 solution by employing a newly elaborated diffusion ordered spectroscopy (DOSY) NMR method hand-in-hand with theoretical calculations.

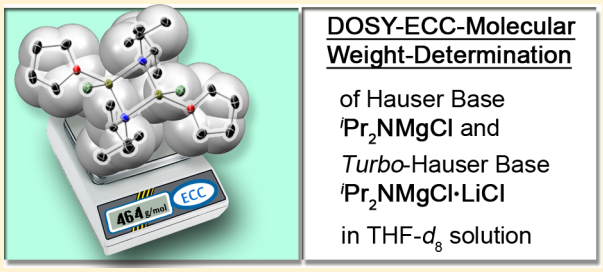

INTRODUCTION

Metalation reactions are one of the most important large-scale synthetic methodologies in chemical industry. Prominent reagents for proton abstraction from organic substrates are organolithium reagents like *n*-butyllithium closely followed by sterically demanding amides like diisopropylamide, LDA; 1,1,1,3,3,3-hexamethyldisilazide, LiHMDS; and 2,2,6,6-tetramethyl-piperidide, LiTMP.[1] However, the drawback of these strong organic bases is that they often cause competing side reactions, require relatively low temperatures (e.g., −78 to −90 °C), and do not tolerate certain synthetically important functional groups like esters, carbonyls, nitriles, sulfoxides, and halides. This is why in the past decades organomagnesium reagents have found increasing popularity in synthetic chemistry. As compared to organolithium reagents, the magnesium compounds have more covalent character and therefore less reactive metal−ligand bonds. This is why they display a better functional group tolerance and a much greater chemoselectivity. In the late 1940s, Hauser and co-workers succeeded in the development of the amido Grignard reagents R_2NMgCl, formally known as Hauser bases, by replacing the alkyl ligand of a Grignard reagent with a secondary amide.[2] The breakthrough in the synthetic application of Hauser bases ensued in the 1980s and 1990s, where Eaton and co-workers introduced $^{i}Pr_2N$- and TMPMgBr, which were shown to *ortho*-magnesiate carboxamides.[3] Later, Kondo, Sakamoto, and co-workers reported the utility of $^{i}Pr_2NMgX$ (X = Cl, Br) as selective deprotonation reagents for heterocyclic thiophene (exclusively at the 2- position) and phenylsulphonyl-substituted indoles.[4] In 2006, Knochel and co-workers developed the mixed lithium and magnesium amide bases $R_1R_2NMgCl{\cdot}LiCl$. These so-called *Turbo*-Hauser bases display a better solubility and a higher reactivity for the magnesiation of various functionalized (hetero)aromatic compounds.[5] Although there is a great deal of information on the utility of these reagents, very little is known regarding the nature of (*Turbo*-)Hauser bases in solution. One reason for that paucity is the complex and interlocked equilibrium framework in solution that Hauser bases show. It was proposed that it could be similar to the Schlenk-equilibrium of Grignard reagents in ether solution, where more than one magnesium-containing species exists.[6] A rearrangement of the organic ligand takes place and ends up in an equilibrium with the diorganomagnesium and the magnesiumdihalide (eq 1 in Scheme 1).[7] Later, molecular association studies also revealed oligomeric Grignard structures in diethyl ether. This fact further complicated the simple Schlenk-equilibrium (eq 1) as oligomeric species had to be included in an advanced pattern (eq 2 in Scheme 1).[8] There are a few known solid-state structures of Grignard complexes.[9] It was found that the Mg atoms are predominantly tetrahedrally coordinated in the solid state and dimeric species are bridged through halide atoms. Especially in the late 1960s, a lot of solution structure investigations have been done mainly by ebullioscopic,[8,10] calorimetric,[11] and NMR-[12] measurements. The position of the Schlenk-equilibrium is considered to be

Received: January 11, 2016
Published: March 24, 2016

DOI: 10.1021/jacs.6b00345
J. Am. Chem. Soc. 2016, 138, 4796−4806

Scheme 1. Schlenk-Equilibrium

"Common" Schlenk-equilibrium

$$2\ RMgX \overset{K_s}{\rightleftharpoons} R_2Mg + MgX_2 \qquad (1)$$

"Advanced" Schlenk-equilibrium

$$\text{oligomer} \rightleftharpoons (RMgX)_2 \rightleftharpoons 2\ RMgX \qquad (2)$$

$$R_2Mg{\cdot}MgX_2 \rightleftharpoons R_2Mg + MgX_2$$

dependent on the concentration, the nature of the solvent, the steric demand of the organic substituent, the halide involved, and the temperature.[13] In THF, all alkyl and arylmagnesium halides (Cl, Br, I) are found to be monomeric over a wide concentration range.[8,11] In diethyl ether, alkyl and aryl Grignard reagents are mostly monomeric at low concentrations (less than 0.5 M) and mostly dimeric at higher concentrations (0.5–1.0 M).[10a] However, to our own surprise, there are no investigations about the aggregation of Hauser bases in solution. Only one study on the solution structure of *Turbo*-Hauser base **2** and its bulky analogue TMPMgCl·LiCl exists.[14] Unfortunately, the exact nature of the solution species could not be identified because the employed diffusion coefficient-formula weight (D-FW) analysis[15] that is based on an internal calibration curve (ICC, pioneered by Williard et al.[16]) lacks the required accuracy. Many internal standards, which might interfere with the reactive metal complexes, are required. Recently, we developed a novel DOSY-NMR method for accurate molecular weight (MW) determination that rests on external calibration curves (ECC) with normalized diffusion coefficients. One internal reference is sufficient, so the addition of multiple internal references is not required anymore. This method offers independent of diversities in temperature or viscosity an easy adjustment on the analyte geometry and a robust access to determine accurate MWs in solution with an error of better than ±9% (for more information, see the Supporting Information).[17] Using this method, we were already able to characterize the complex oligomeric mixture of LDA in toluene solution.[18] Hence, we embarked to apply our newly developed and improved NMR techniques to identify reactive organometallic species in solution.[19] In cases where an unequivocal assignment is impossible, given the existence of structural isomers, we have complemented the experimental findings with electronic structure calculations. The latter also provide further insight into the aggregation patterns in solution. Understanding how (*Turbo*-)Hauser bases self-organize and interact among each other, especially in solution where they operate, is a premium in structure–reactivity elucidation.

RESULTS

Solid-State Structure of $^{i}Pr_2NMgCl$ 1. To shed light on the solution structure of **1**, we first synthesized the prominent Hauser base $^{i}Pr_2NMgCl$ **1** and crystallized it from a THF/toluene 1:1 mixture at −6 °C (see Experimental Section).[20] The crystal structure of **1** is shown in Figure 1. TMP[21] and HMDS[22] Hauser bases alike all Grignard dimers[9a,b,e,23] show the halides in the bridging position in the solid state (like **D2** in category B from Chart 1). In contrast, **1** dimerizes featuring the amido ligands in the bridging position (**D1** in category A from Chart 1). Searching the Cambridge Crystallography Database for Hauser bases reveals that there are only three other dimeric

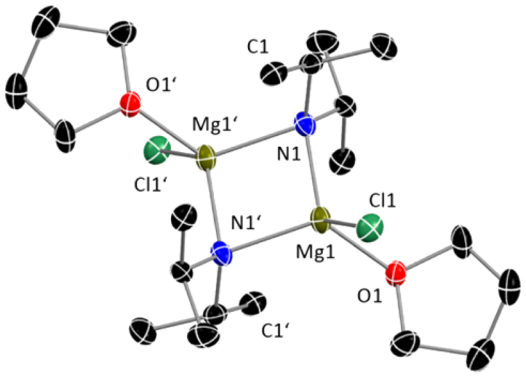

Figure 1. Solid-state structure of $[\mathbf{1}{\cdot}THF]_2$ (**D1**) with hydrogen atoms and disorder omitted for clarity (selected bond lengths and angles are displayed in Figure S1).

Chart 1. Most Plausible Aggregation Modes of $^{i}Pr_2NMgCl$ 1 in THF-d_8 Solution[26]

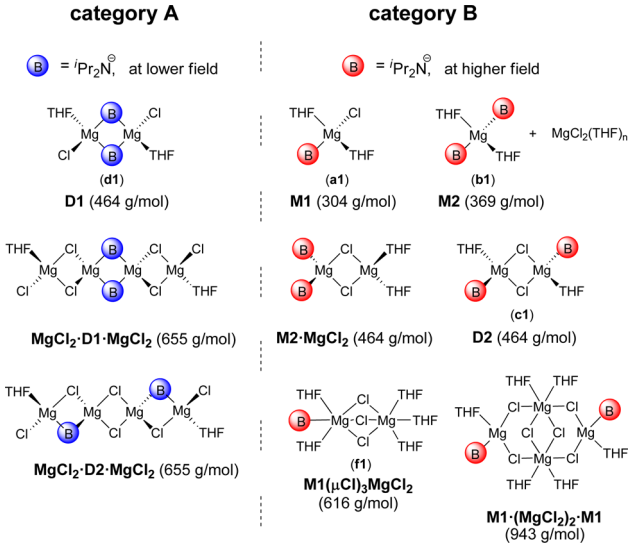

amido bridged Hauser bases in the literature.[24] All have one feature in common: less bulky amido ligands like Et_2N^-,[22a] $Ph_3P{=}N^-$,[25] and $^{i}Pr_2N^-$[14] in the bridging position. It can be concluded that in the solid state the switch from the halide to the amido bridge seems advantageous.[6] However, solid-state structures may not necessarily be maintained in solution.

Solution Structure of $^{i}Pr_2NMgCl$ 1. In synthesis, organometallic compounds are predominantly used in solution. Therefore, we were interested in the solution structure of **1**. The most plausible aggregation modes of a Hauser base in THF solution are filed in Chart 1. A dissolved crystal of **1** in THF can either retain its dimeric status **D1** or isomerize to the chloride bridged dimer **D2.** On the other hand, these dimers can dissociate to the monomer **M1** or rearrange according to the Schlenk-equilibrium to the diamidomagnesium **M2** and $MgCl_2$. When an excess of $MgCl_2$ is present, $MgCl_2$ salt cocoordinated species like $\mathbf{M1}(\mu\mathbf{Cl})_3\mathbf{MgCl_2}$, $\mathbf{M2{\cdot}MgCl_2}$, $\mathbf{MgCl_2{\cdot}D1(D2){\cdot}MgCl_2}$, or $\mathbf{M1{\cdot}(MgCl_2)_2{\cdot}M1}$ might also be present in solution. All of the mentioned species can be distinguished either by their MW or additionally by the chemical environment of the isopropyl groups that is reflected in the chemical shift δ. As compared to terminal amido ligands (category B, Chart 1), the bridging ones (category A, Chart 1)

DOI: 10.1021/jacs.6b00345
J. Am. Chem. Soc. 2016, 138, 4796–4806

show a significant low field shift due to the presence of additional electron-withdrawing metals.

At room temperature, however, the ^{1}H NMR spectrum of **1** (Figure 2) shows one broad signal set corresponding to a single

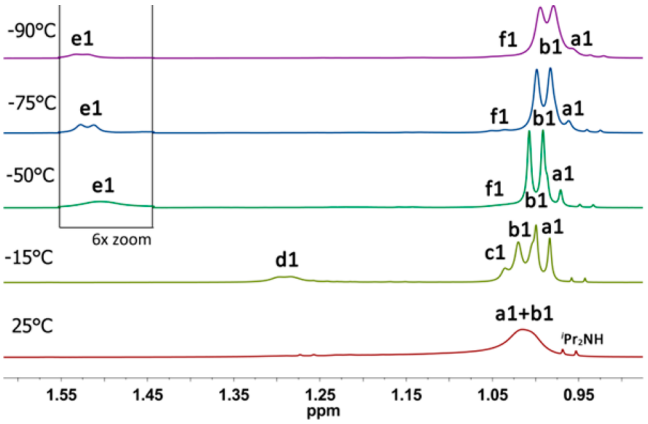

Figure 2. Superposition of ^{1}H NMR spectra of crystalline $[\mathbf{1}\cdot THF]_2$ (0.10 M, $-CH_3$ region) redissolved in THF-d_8 at various temperatures. Assignment of signals: see Scheme 2.

species **a1** at high field (2.94/1.01 ppm for α-CH/CH_3, Chart 1, category B). The ^{1}H DOSY-ECC-MW-determination agrees best with the heteroleptic monomer **M1** (MW_{calc} = 304 g/mol, MW_{det} = 310 g/mol, MW_{err} = −2%),[27] while dimeric **D2**, **M2·MgCl$_2$**, and bigger aggregates can be excluded ($MW_{err} \geq 33\%$). Below 0 °C, two additional species **b1** (3.10/1.02 ppm, category B), **c1** (3.24/1.01 ppm, category B) at high field and **d1** at low field (3.43/1.29 ppm, category A) grow in. From NMR studies on alkyl Grignard reagents it is known that homoleptic dialkylmagnesium monomers analogue **M2** resonate at lower field than heteroleptic monomers analogue **M1**.[28] In fact, MW-determination for species **b1** agrees perfectly with the homoleptic diamidomagnesium **M2** (MW_{calc} = 369 g/mol, MW_{det} = 356, MW_{err} = 4%). The MW of **c1** matches to those of dimeric **D2** and **M2·MgCl$_2$** (MW_{calc} = 464 g/mol, MW_{det} = 450 g/mol, MW_{err} = 3%) that have the same MW. Both have a comparable chemical and magnetic environment and cannot be distinguished by their MWs. Both species could be present in solution, but it is most likely that the equilibrium is significantly shifted to the side of dimer **D2** because it displays less steric hindrance as compared to **M2·MgCl$_2$**. To investigate the structure of the dimer in solution, electronic structure calculations were carried out on the possible isomers. The latter were performed with the B3LYP-D3 method,[29] including solvent corrections. Further information can be found in the Computational Details. Free energy differences confirm **M2·MgCl$_2$** to be disfavored relative to the **D2** species by 53.1 kJ/mol (Table S29). The most stable structure found corresponds in fact to a *cis*-isomer of **D2**, with both bases orientated to the same side of the Mg_2Cl_2 ring. This arrangement optimizes dispersion interactions between both the propyl moieties and the THF rings on each side. The *trans* configuration is slightly higher in energy by 7.2 kJ/mol. However, this marginal difference is not to be taken for granted because weak interactions with the solvent (which in our computations is only included as a dielectric continuum) could easily counterbalance this effect. The optimized structure of **M2·MgCl$_2$** shows a large N−Mg−N angle of about 146° (Figure S35), illustrating the steric strain of both diisopropylamido groups when coordinated to the same metal center adding to the energetic disfavor. Species **d1**, with the highly low field shifted signal, is in good agreement with the amido bridged dimer **D1** (MW_{calc} = 464 g/mol, MW_{det} = 435 g/mol, MW_{err} = 6%) that is similar to the crystal structure of $[\mathbf{1}\cdot THF]_2$ (Figure 1). Lowering the temperature dramatically influences the position of the Schlenk-equilibrium of Hauser base **1** (Scheme 2). While

Scheme 2. Determined Composition of Hauser Base ^{i}Pr$_2$NMgCl 1 in THF-d_8 Solution[a]

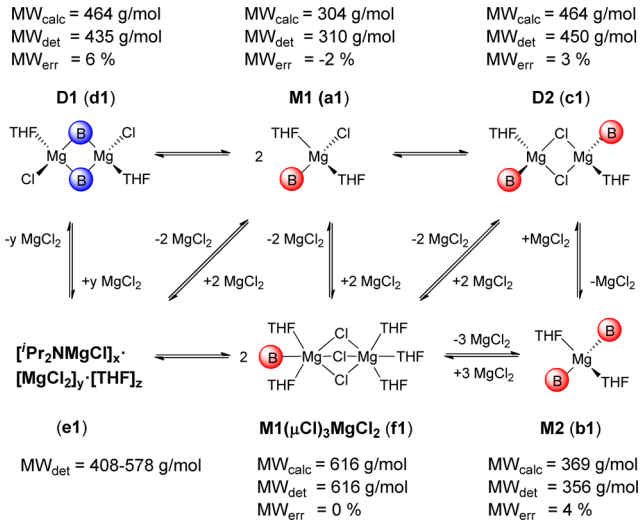

[a]The MWs were derived from ^{1}H DOSY-ECC-MW-determinations.[26] The accuracy of this method is in the range of $MW_{err} < \pm 9\%$.[17,35]

at room temperature, the monomer **M1**/**M2** ratio is 4:1, this ratio switches completely at −75 °C to the ratio of 1:4 (Table 1, 0.100 M). The huge population of homoleptic monomer **M2**

Table 1. Schlenk-Equilibrium "Constant"[a] K_s for the Reaction $(^iPr_2N)_2Mg$ (M2) + $MgCl_2$ ⇌ $2\,^iPr_2NMgCl$ (M1)

T/°C	K_s (0.015 M)	K_s (0.100 M)
25	25.00	16.00
0	8.16	4.43
−15	2.97	1.49
−25	1.00	0.68
−50	0.18	0.10
−75	0.12	0.05

[a]Usually the Schlenk-equilibrium constant K_s is derived from ^{1}H integrals of α-CH protons with $K_s = [^iPr_2NMgCl]^2/[(^iPr_2N)_2Mg]^2$ with the approximation: $[(^iPr_2N)_2Mg] \approx [MgCl_2]$. However, our results show that the concentration of $(^iPr_2N)_2Mg$ is not equal to $MgCl_2$ because the latter is involved in further reactions with Hauser base **1**. This is also reflected in our determined K_s values that show therefore concentration dependence.

at low temperatures is in good agreement with the work of Smith and Becker who showed that the formation of RMgCl from R_2Mg and $MgCl_2$ is endothermic in THF solution.[11] The same seems valid for Hauser base **1**. The equilibrium constants of the Schlenk-equilibrium summarized in Table 1 display the equilibrium to move to homoleptic **M2** + $MgCl_2$ with increasing concentration and decreasing temperature. The formation of **M2** is accompanied by the release of free $MgCl_2$ to the solution, most probably as a monomer with up to four THF molecules.[30] Therefore, it might not be surprising when

DOI: 10.1021/jacs.6b00345
J. Am. Chem. Soc. 2016, 138, 4796−4806

free magnesium dihalide coordinates to some complexes at low temperatures. At −50 °C, dimers **D1** (**d1**) and **D2** (**c1**) dissipate at the expense of two new species **e1** (3.39/1.50 ppm, category A) and **f1** (3.21/1.04 ppm, category B) that display an even more pronounced low field shift. This remarkable shift can be attributed to an additional coordination of $MgCl_2$ to **M1**, **D1**, or **D2**. When $MgCl_2$ coordinates to monomer **M1**, then a structure like **M1**(μCl)$_3$**MgCl$_2$** (Chart 1, category B) would be feasible. This coordination mode was suggested for methyl magnesium chloride by Sakamoto and Imamoto et al.[31] With the help of coldspray ionization mass spectrometry (CSI-MS), they proposed that the μ-Cl_3 bridged Grignard reagent was coordinated by four to six THF molecules, whereas the species with five THF molecules was the major component.[31] Additional support is provided by several crystal structures of cationic $[(THF)_3Mg(\mu Cl)_3Mg(THF)_3]^+$ where magnesium chloride is also coordinated in that μ-Cl_3 fashion.[31] Our MW-investigation shows similar results: At −70 °C the ECC-MW-determination gives for signal **f1** a MW of MW_{det} = 512 g/mol that fits **M1**(μCl)$_3$**MgCl$_2$** with four THF molecules (MW_{calc} = 544 g/mol, MW_{det} = 512 g/mol, MW_{err} = 6%). At −80 °C the MW increases significantly to MW_{det} = 616 g/mol that matches perfectly the THF 5-fold solvated **M1**(μCl)$_3$**MgCl$_2$** (MW_{calc} = 616 g/mol, MW_{det} = 616 g/mol, MW_{err} = 0%), indicating that a higher solvation is favored at lower temperatures.[32] In the literature there are several crystal structures known of the type **M1**·(**MgCl$_2$**)$_2$·**M1** (see Chart 1, category B), where two monomers **M1** are bridged by two magnesium dichlorides in an open cubic aggregation mode.[31,33] However, it seems that the dissociation into smaller parts is favored over that open cubic arrangement in solution of **1** (MW_{calc} = 943 g/mol, MW_{det} = 616 g/mol, MW_{err} = 35%), which was already proposed by D. Seyferth in 2009.[13] Additionally to **f1**, species **e1** appears at much lower field (category A). The ECC-MW-determination shows a temperature-dependent MW distribution (MW_{det} = 409 g/mol at −50 °C, 446 g/mol at −70 °C, and 578 g/mol at −80 °C). The addition of $MgCl_2$ to dimers **D1** or **D2** would produce aggregates like **MgCl$_2$·D1·MgCl$_2$** or **MgCl$_2$·D2·MgCl$_2$** (Chart 1, category A). However, several other $MgCl_2$ coordinated, amido bridged species would also be conceivable. Unfortunately, in the literature there are no crystal structures of $MgCl_2$ coordinated, ligand bridged Hauser bases or Grignard reagents that could provide a hint to the most plausible aggregates. The high MW of 578 g/mol at −80 °C gives much room for interpretation. This is why we can only speculate how the composition of aggregate **e1** could look like. Noticeable is that in contrast to all other species, the $-CH_3$ signal of **e1** shifts to lower field with lower temperature (Figure 2). This behavior could be a result of a successive addition of $MgCl_2$ to **D1** or **D2**. At −80 °C the shift to lower field stops,[32] and the MW of **e1** matches dimeric **MgCl$_2$·D1(D2)·MgCl$_2$** (MW_{calc} = 655 g/mol, $MW_{det,corr}$ = 703 g/mol, MW_{err} = −7%, after molar density correction (see Supporting Information section XXXIII)).[34] Although we still cannot be sure about this MW-agreement, it seems that at low temperatures free, monomeric $MgCl_2$ is disadvantageous in solution. Instead, it coordinates to monomeric and/or dimeric RMgCl molecules as discussed for LiCl in the following section.

Solution Structure of ^{i}Pr$_2$NMgCl·LiCl 2. The impact of LiCl on the solution structure of Grignard reagents and Hauser bases is still vigorously discussed. Knochel et al. suggest that LiCl deaggregates RMgX oligomers[5d] and forms a more reactive bimetallic monomer RMgCl·LiCl that is supposed to furnish magnesiate character to the Grignard reagent in the sense of a solvent separated ion pair (SSIP) $[Li(THF)_4]^+[RMg(THF)Cl_2]^-$.[36] Crystallographic evidence of the *Turbo*-Hauser bases TMPMgCl·LiCl[21] (**M1·LiCl**, Chart 2 with B = TMP^-)

Chart 2. Most Plausible Aggregation Modes of ^{i}Pr$_2$NMgCl·LiCl 2 in THF-d_8 Solution[26]

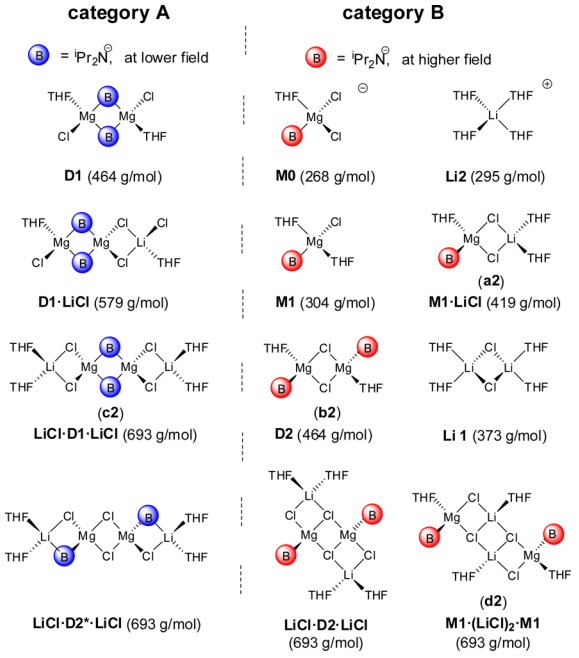

and $[\mathbf{2}\cdot THF]_2$[14] (**LiCl·D1·LiCl**, Chart 2) supports the contact ion pair (CIP) coordination mode in the solid state. Yet still it was not clear whether the mixed metal structure really is maintained in solution or just a transient species. García-Álvarez and Mulvey et al. analyzed[14] crystals of $[\mathbf{2}\cdot THF]_2$ in THF-d_8 solution at −50 °C by employing the ICC D-FW analysis that was pioneered by Li and Williard et al.[16] Because of the lack of appropriate references, the accuracy of the method was not sufficient, and they concluded that they were not able to "clearly establish the exact nature of the solution species".[14] However, the first key conclusion was that the molecular structure of crystalline $[\mathbf{2}\cdot THF]_2$ (**LiCl·D1·LiCl**) was not retained in THF-d_8 solution, and the second was that a SSIP situation like it was proposed by Knochel et al., described by negative charged magnesium ate complexes (like **M0**), and free $[Li(THF)_4]^+$ (**Li2**) seemed most probable (Chart 2, category B).[14] In the following section, we will shed light on the complex solution structure of **2** and prove that both key conclusions have to be revised. Furthermore, we will try to clarify the influence of LiCl on the Schlenk-equilibrium of **1** more generally by applying our accurate DOSY-ECC-MW-determination method[17] and electronic structure calculations.

Primarily, it seems advisible to a priori rationalize which species are feasible to be present in the solution of ^{i}Pr$_2$NMgCl·LiCl **2**. A dissolved crystal of $[\mathbf{2}\cdot THF]_2$ in THF can either retain the coordination **LiCl·D1·LiCl** or isomerize to **LiCl·D2*·LiCl** (Chart 2, category A). In the first aggregation mode, the isopropyl groups are neighbored by compact chloride ligands, enabling a free rotation of the isopropyl groups, whereas in the latter they are neighbored to a sterically demanding THF molecule that would result in a steric

DOI: 10.1021/jacs.6b00345
J. Am. Chem. Soc. 2016, 138, 4796−4806

repulsion. This is why we suggest that species **LiCl·D1·LiCl** should be highly favored over **LiCl·D2*·LiCl**.

This again is supported by our calculations (Table S31). The free energy difference between **LiCl·D1·LiCl** and **LiCl·D2*·LiCl** is 55−56 kJ/mol (the former being more stable) in the temperature range from −90 to +25 °C. Inspection of the optimized structures confirms the steric hindrance (Figure S38). In the **LiCl·D1·LiCl** structure the Mg^{2+} cations are aligned with the Li^+, resulting in a high-symmetric structure with a close to tetrahedral coordination at each metal atom. In the **LiCl·D2*·LiCl** case the Li^+ cations are forced out of this axis to accommodate the isopropyl groups at both ends. Another possibility is that the dimer of $[\mathbf{2}\cdot THF]_2$ can dissociate into monomeric units **M1·LiCl**. These monomers could recombine via a four-membered $[MgCl]_2$ ring (**LiCl·D2·LiCl**) or by a smaller $[LiCl]_2$ ring (**M1·(LiCl)$_2$·M1**) in the center. It is also possible that LiCl dissociates as a well-known dimer[37] $[(THF)_2Li(\mu Cl)_2Li(THF)_2]$ **Li1** to produce LiCl-free species **M1**, **D1**, or **D2** or that lithium dissociates as a solvent separated ion pair $[Li(THF)_4]^+$ **Li2** that would produce an SSIP ate-complex like **M0**, where two chlorides are coordinated to the magnesium ion (Chart 2, category B). The ^{7}Li spectra at RT show a singlet at 0.18 ppm (25 °C) that shifts to lower field with decreasing temperature (0.38 ppm at −100 °C, Figure 3).

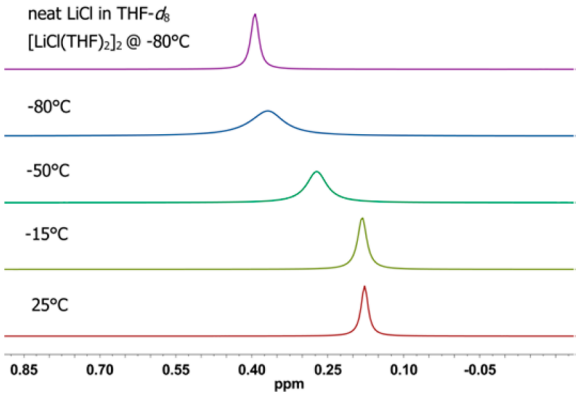

Figure 3. Superposition of ^{7}Li NMR spectra[39] of crystalline $[\mathbf{2}\cdot THF]_2$ (0.1 M) redissolved in THF-d_8 at various temperatures. On the top: ^{7}Li-spectrum of neat **Li1** in THF-d_8 at −80 °C.

The presence of LDA, where lithium coordinates directly to the diisopropyl amide, can therefore be excluded because LDA resonates in the ^{7}Li NMR experiment temperature independently at about 2.0 ppm (Figure S14). Additionally, the solvent separated cation $[Li(THF)_4]^+$ **Li2** can be excluded to be populated at detectable concentrations too, because it is known that the solvent separated lithium ion **Li2** resonances are at a negative chemical shift (−1.1 ppm in THF).[38]

Further support is provided by the crystal structure of $[\mathbf{2}\cdot THF]_2$ where the lithium cation is located close to the isopropyl groups in a middle distance of 4.49 Å to the closest CH_3-protons.[21] This relatively close distance should be detectable in a ^{1}H-^{7}Li-HOESY experiment,[19e] when lithium is coordinated next to the magnesium amide. In fact, the ^{1}H-^{7}Li-HOESY spectra show at high temperatures a cross peak between the ^{7}Li signal and the CH_3 signals of species **a2**, **b2**, and **c2** (Figure S9), indicating that lithium does coordinate to Hauser base **1**. At room temperature, two different species (**a2**, 2.92/1.03 ppm, category B; and **c2**, 3.42/1.33 ppm, category A) can be identified in the ^{1}H NMR spectrum of $[\mathbf{2}\cdot THF]_2$ (Figure 4). The MW-determination of **a2** gives at all temperatures a MW that fits almost perfectly the LiCl

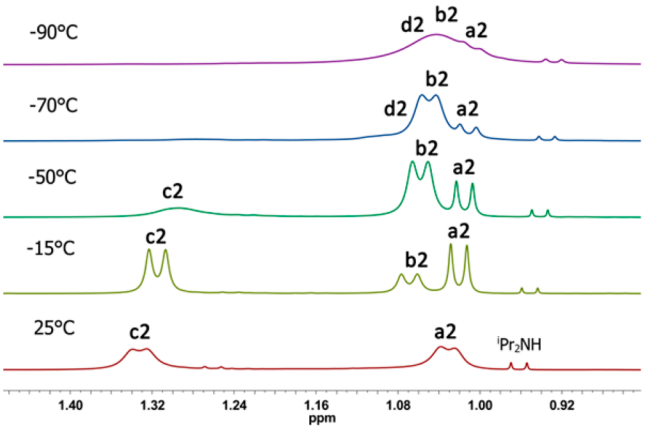

Figure 4. Superposition of ^{1}H NMR spectra of crystalline $[\mathbf{2}\cdot THF]_2$ (0.1 M, $-CH_3$ region) redissolved in THF-d_8 at various temperatures.

coordinated monomer **M1·LiCl** (MW_{calc} = 419 g/mol, MW_{det} = 425 g/mol, MW_{err} = −2%). As compared to the salt-free monomer **M1** (**a1**), the metal chloride cocoordinated monomers **M1(μCl)$_3$MgCl$_2$** (**f1**) and **M1·LiCl** (**a2**) are shifted to lower field ($\Delta\delta \approx 0.02$ ppm), due to an additional electron-withdrawing metal chloride coordinated to the aggregate. The same is true for signal **c2** that appears at the dimer region of **D1** (Chart 2, category A) but also low field shifted by 0.02 ppm (as compared to LiCl-free dimer **D1**), indicating that **c2** is due to the LiCl cocoordinated dimer **LiCl·D1·LiCl**. At 25 °C, the determined MW of **c2** (MW_{calc} = 693 g/mol, MW_{det} = 525 g/mol, MW_{err} = 24%) is smaller than expected. Yet with decreasing temperature, the MW grows significantly (MW_{det} = 598 g/mol at −15 °C, 618 g/mol at −40 °C, and 635 g/mol at −50 °C) until it stops growing further at −60 °C (MW_{det} = 661 g/mol). The same trend was already observed for species **MgCl$_2$·D1(D2)·MgCl$_2$** (**e1**) of Hauser base **1**. In contrast to all other species of **2**, the α-CH signal of **c2** shifts like **e1** to lower field with lower temperature (Figure S6). This is why a successive coordination of LiCl to **D1** could again explain this behavior (25 to −40 °C: av MW_{det} = 582 g/mol, MW_{calc}(**D1·LiCl**) = 579 g/mol, MW_{err} = −1%).[40] Finally, between −60 and −70 °C, it is possible to determine the MW of tetranuclear dimer **LiCl·D1·LiCl** (**c2**) as two lithium chlorides coordinated to dimer **D1** (MW_{calc} = 693 g/mol, MW_{det} = 661 g/mol, MW_{err} = 5%). A monomer−dimer equilibrium of **a2** and **c2** was already suggested by García-Álvarez and Mulvey et al.[14] Concentration experiments showed that species **a2** dominates at lower concentrations, whereas **c2** is mostly populated at higher concentrations.[14] Below −70 °C, the solubility limit is reached and signal **c2** disappears. With decreasing temperature, a third species next to **a2** forms (**b2**: 3.13/1.07 ppm, category B). Further cooling results in a shift of the oligomer equilibrium. The integral of **b2** increases significantly at the expense of **a2** and **c2**. The MW-determination of **b2** offers at all temperatures a MW that fits the LiCl free dimer **D2** (MW_{calc} = 464 g/mol, MW_{det} = 461 g/mol, MW_{err} = 1%). The ^{1}H-^{7}Li HOESY experiment indicates at 0 °C the interaction of **b2** with the lithium cation. However, the cross peak vanishes at lower temperatures when **b2** becomes the most populated species, indicating that **b2** would not coordinate strongly to LiCl. At −70 °C, next to **b2**, a fourth species **d2** is detectable in the ^{1}H

DOI: 10.1021/jacs.6b00345
J. Am. Chem. Soc. 2016, 138, 4796−4806

experiment. At −100 °C, species **d2** can be deconvoluted in the DOSY NMR experiment (Figure S31), giving a MW_{det} value that fits to LiCl coordinated species **LiCl·D2·LiCl/M1·(LiCl)$_2$·M1** (**d2**) (MW_{calc} = 693 g/mol, MW_{det} = 641 g/mol, MW_{err} = 7%).[41] The ^{7}Li DOSY-ECC-MW-determination experiments give further information about the aggregation behavior of **2**. All species produce only one signal that broadens and shifts to lower field with decreasing temperature (Figure 3). Only at 0 °C there is a small shoulder at the ^{7}Li-signal, verifying that more than one Li species is present in solution of **2**. From 25 to −40 °C, the ^{7}Li DOSY-ECC-MW-determination gives an average, temperature-dependent MW, that reflects an average value produced by all three lithium aggregates (MW_{det} = 454−496 g/mol). Below −60 °C the MW decreases significantly without further change (MW_{det} = 382 g/mol from −60 to −100 °C). This can be attributed to first **LiCl·D1·LiCl** (**c2**), precipitating from solution and the concentration of **M1·LiCl** (**a2**) decreasing significantly to very small amounts, and finally to the residual lithium chloride present in solution as the well-known [(THF)$_2$Li(μCl)$_2$Li(THF)$_2$]-dimer **Li1** (MW_{calc} = 373 g/mol, MW_{det} = 382 g/mol, MW_{err} = −2%) that becomes the most populated Li-species at low temperatures.[42] The formation of significant amounts of **Li1** is also reflected in the chemical shift of the ^{7}Li nucleus. With decreasing temperature the **Li1** concentration increases. This is why the ^{7}Li signal moves toward the chemical shift of the LiCl dimer **Li1** (Figure 3).[43] Additionally, the signal gets very broad. The reason for that will be discussed in the following section.

DISCUSSION

At low temperature the decreased solubility could be one reason for the ^{7}Li signal broadening. Additionally, we think that the formation of **LiCl·D2·LiCl/M1·(LiCl)$_2$·M1** from the reaction of LiCl (**Li1**) and dimer **D2** has even a bigger impact on the signal broadening, because the chemical environment of lithium in **LiCl·D2·LiCl/M1·(LiCl)$_2$·M1** differs from that in **Li1**. Yet, how would the reaction of **Li1** with **D2** occur? We already proposed the tetrameric structures **LiCl·D2·LiCl** and **M1·(LiCl)$_2$·M1** (Chart 2) as products. In both structures, two chlorides at the magnesium atoms show a coordination number of three. Searching the Cambridge Crystallography Database[44] reveals that magnesium chlorides, with a μ-Cl$_3$ coordination, predominantly form cubic aggregation modes in the solid state.[33,45] Bickelhaupt and Solà et al. have shown that the most stable isomer of methylmagnesium chloride is a T_d-symmetric $(CH_3MgCl)_4$ tetranuclear cluster with a cubic $(MgCl)_4$ core and terminal CH_3 groups at the magnesium vertexes.[46] Li halides are also known to build stable cubic tetramers $[LiX]_4$ (X = Cl, Br, I)[47] and even heteroleptic cubanes in the solid state (see compound **3** in Figure 5).[48] This is why the interaction of the LiCl-dimer **Li1** with dimer **D2** to a cubic transition state structure is most feasible. Because the ring sizes of $[LiCl]_2$ and $[MgCl]_2$ differ, a fast dissociation of the cubane back to the corresponding dimers would be plausible. Once the cubane is formed, it could open on one side to produce the already mentioned aggregates **LiCl·D2·LiCl** with a $[MgCl]_2$ core and **M1·(LiCl)$_2$·M1** with a $[LiCl]_2$ core (Scheme 4). There is evidence for an opened $[LiCl]_4$ cube already.[47d] To find out which of those structures is the most stable in solution, we carried out further calculations (vide infra). Additional support for the interaction of **Li1** with **D2** is provided by the absence of LiCl-free species **M1** (MW_{calc} = 304 g/mol) and homoleptic diamidomagnesium **M2** (MW_{calc} = 369 g/mol, see Chart 1, MW_{det} (all species) = 425−661 g/mol, $MW_{err} \geq 28\%$, and $MW_{err} \geq 13\%$). At low temperatures **M2** is the main species in the solution of Hauser base **1**. Ashby et al. proposed for the formation of **M2** a dimer-based mechanism (see Scheme 3A).[10a] A rearrangement of dimer **aII** to an asymmetric dimer **aIII** forms two excellent leaving groups, which dissociate into the corresponding diorgano magnesium R_2Mg and $MgCl_2$ (**aIV** in Scheme 3A). In the presence of LiCl, it is possible to rationalize several structures like **bI**−**bVIII**. Interestingly, in those structures, the LiCl coordinated monomer **bI**, the LiCl-dimer **bII**, and dimeric **bIII** represent always the best leaving groups (Scheme 3B), especially at low temperatures where monomeric LiCl and **M1** are highly unfavorable. Further, the cleavage of $MgCl_2$ or R_2Mg would be accompanied by a release of solvent separated ions that would be very unlikely because no solvent separated species are observable in solution of

Scheme 3. (A) Mechanism on the Formation of R_2Mg and $MgCl_2$ via an Asymmetric Dimer aIII Proposed by Ashby; and (B) In the Presence of LiCl in Various Aggregation Modes of 2, bI, bII, and bIII are Always the Best Leaving Groups, Suppressing the Formation of Homoleptic R_2Mg and $MgCl_2$ aIV[a]

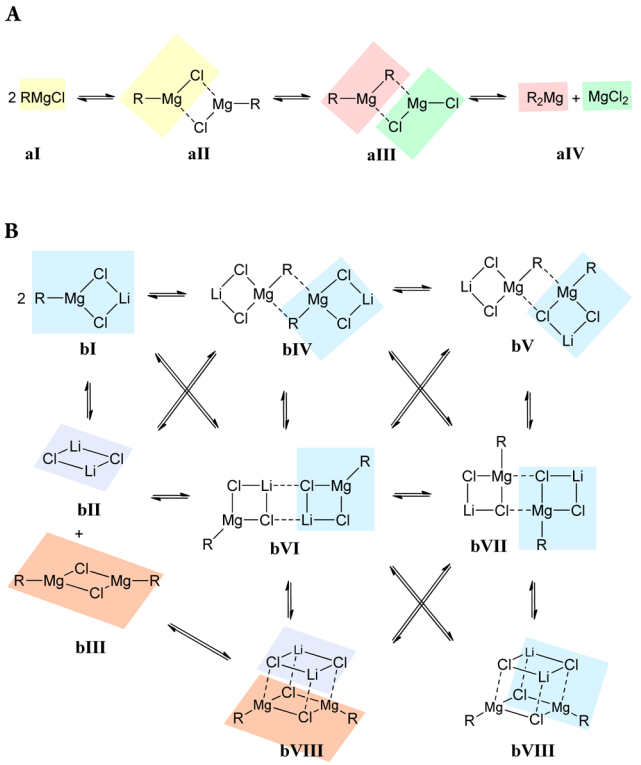

[a]Any solvation was omitted for clarity.

3 Ar = 2,6-Pmp$_2$C$_6$H$_3$

Figure 5. An equimolar reaction of $[2,6\text{-Pmp}_2C_6H_3Li]_2$ (Pmp = 2,3,4,5,6-Me$_5$C$_6$) with CdI_2 and crystallization from a saturated hexane solution at −30 °C yields crystals of cubane **3**.[48a]

DOI: 10.1021/jacs.6b00345
J. Am. Chem. Soc. 2016, 138, 4796−4806

Hauser base **1** and **2**.[49] If the LiCl dimer **Li1** (**bII**) would not communicate with dimer **D2** (**bIII**), then the formation of homoleptic **M2** (**aIV**) should be observable, which is not the case. Without LiCl, the dimer **D2** is only stable above −50 °C. Yet with LiCl, it is the main species below −50 °C in Hauser base **2** most probably because of its interaction with the LiCl dimer **Li1**. This contrasting behavior could be reflected in the different aggregation modes of LiCl and $MgCl_2$ in THF solution. The former is predominantly dimeric, enabling a sufficient overlap of the $[LiCl]_2$ ring with dimer **D2**, while $MgCl_2$ is predominantly monomeric.[30b] This is why $MgCl_2$ stabilizes more efficiently in a terminal coordination mode like in **M1**(μCl)$_3$**MgCl$_2$** and **MgCl$_2$·D1(D2)·MgCl$_2$**. To address some of the open questions regarding the interaction of **Li1** and **D2** in THF solution, we carried out further calculations on the complexes. We started by computing the relative free energies for **M1·(LiCl)$_2$·M1** and **LiCl·D2·LiCl** (depicted in Scheme 4). Our results show that the ladder and boat

Scheme 4. Proposed Interaction of the LiCl Dimer Li 1 with the Hauser Base Dimer D2

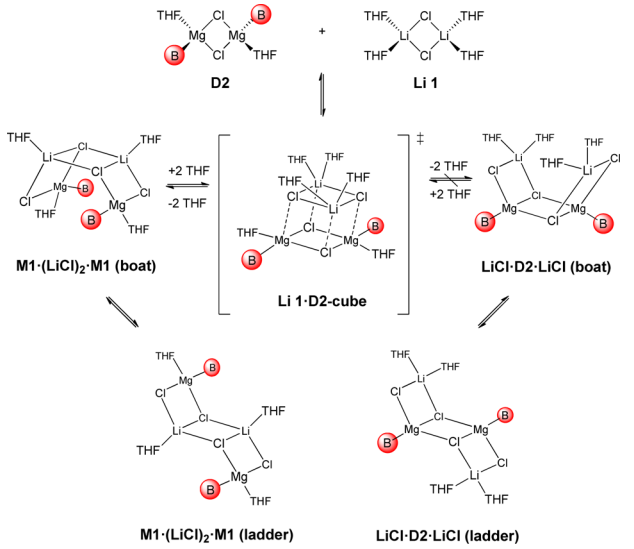

configurations, both for the **M1·(LiCl)$_2$·M1** and for the **LiCl·D2·LiCl** isomers, are very close in energy (Table S31) with differences below 3 kJ/mol (at 25 °C). This is definitely within the uncertainty of the method and would indicate no particular conformational preference. However, the structures **M1·(LiCl)$_2$·M1** with an inner $[LiCl]_2$ four-membered ring are favored by 42.2 kJ/mol in free energy. The next question is whether the formation of **M1·(LiCl)$_2$·M1** is favored in solution as well. This complex can be formed, for example, by the reaction of **D2** with **Li1** (eq 3) or by dimerization of two **M1·LiCl** molecules (eq 4, Scheme 5).

The free energies for the mixed Li−Mg dimer formation were computed in a range from −90 to +25 °C, revealing that the dimerization process of **D2** and **Li1** (eq 3) to give **M1·(LiCl)$_2$·M1** is slightly exergonic (−3.3 to −14.3 kJ/mol, from lower to higher temperature, Table S33). Species **M1·(LiCl)$_2$·M1** could, as such, be formed in the solution of *Turbo*-Hauser base **2**. In contrast, the dimerization of two **M1·LiCl** molecules (eq 4) is unfavored due to an endergonic reaction (17.3 to 3.9 kJ/mol, Table S35). Obviously such values have to be considered with certain reservations because the molarity is changing (formally, two THF molecules are released into

Scheme 5. Free Energies Computed in a Range from −90 to +25 °C

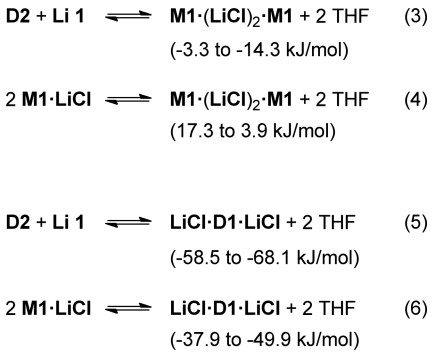

solution during the process, so we are dealing with the formation of 3 molecules from 2 starting products). The quantum chemical result is, therefore, strongly influenced by the translation entropy. In the gas phase, the latter can be computed from the harmonic vibrational partition function. This does not apply to the solution, because solvated molecules are not free to move and possess lower translational entropy than in the gas. Our results already include a correction as suggested by Ardura et al. on the basis of a cell model for the change in translational degrees of freedom.[50] However, this little energy gain for the formation of **M1·(LiCl)$_2$·M1** stays in good agreement with our NMR experiments, showing that **D2** and **Li1** interact and communicate with each other but still the equilibrium is highly on the side of free **D2** and **Li1**. In tune with the crystal structure of **2**, the highest energy gain was identified for the formation of **LiCl·D1·LiCl** (**c2**) (eqs 5 and 6 in Scheme 5). Again, the reaction of **D2** and **Li1** is preferred over the dimerization of two **M1·LiCl** molecules by 19.4 kJ/mol.[51] Interestingly, the solubility limit of **LiCl·D1·LiCl** is reached at approximately −70 °C, providing small amounts of **M1·(LiCl)$_2$·M1** that is thermodynamically less stable. One additional open question is the existence of cubic intermediates through which the larger mixed Li−Mg aggregates could be formed. Because there are no experimental data available on such transient species, one can only postulate about different coordination motifs. We considered four possible cubane structures **Li1·D2-cube** (**A**−**D**) with two available coordination sites at each Li and an additional two at each Mg site (Figure 6). Our calculations clearly identify complexes **B** and **C** as the most unstable, given the low coordination number of the Mg sites (Table S30).

A direct comparison can be in fact established between **Li1·D2-cube** (**A**) and **Li1·D2-cube** (**B**), with **A** being favored over **B** in the considered temperature range by about 10 kJ/mol. For the preferred cubane structures **A** and **D**, one might consider the associated equilibria given by the general equations:

$$\mathbf{D2} + \mathbf{Li1} \rightleftharpoons \mathbf{LiCl{\cdot}D2\text{-}cube} + n\mathrm{THF} \quad (7)$$

$$2\mathbf{M1{\cdot}LiCl} \rightleftharpoons \mathbf{LiCl{\cdot}D2\text{-}cube} + n\mathrm{THF} \quad (8)$$

with n = 0 for **D** and 2 for **A**. As mentioned before, the change in molarity is an obstacle in computing the free energies. By considering two equilibria simultaneously, where in one case the molarity change entropically promotes the products (**A**) and in the other the reactants (**D**), the computed free energies for dimerization according to equilibrium 7 are given in Figure 7 (Table S32). The dimerization of two **M1·LiCl** molecules to

DOI: 10.1021/jacs.6b00345
J. Am. Chem. Soc. 2016, 138, 4796−4806

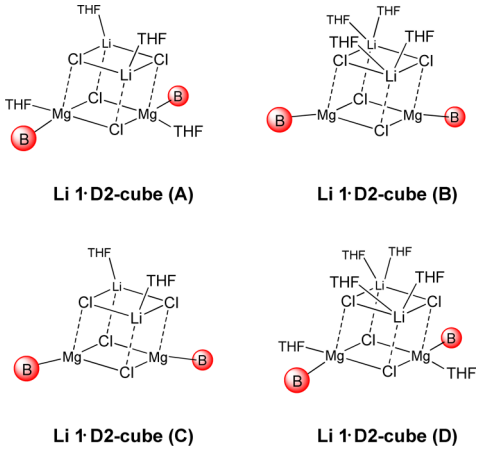

Figure 6. Overview of possible cube structures of *Turbo*-Hauser base **2**.

form **Li1·D2-cube (A–D)** (eq 8) is on average 19.4 kJ/mol higher in energy (Table S34).

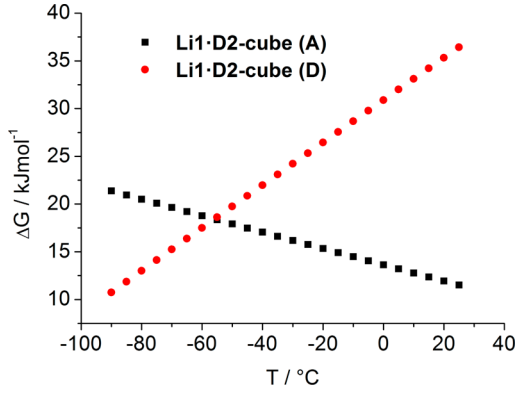

Figure 7. Computed free energies for dimerization of **D2** + **Li1** to give **LiCl·D2-cube (A)** and **LiCl·D2-cube (D)**.

As expected, the formation of complex **D** would be most favorable at lower temperatures. The crossing point is at about −55 °C. Although the equilibrium is always shifted toward the reactants, the differences can be relatively small, as low as 10.7 kJ/mol, such that the cubic intermediate should be accessible, even if not stable relative to the metal dimer complexes **D2** and **Li1**. Our results show that the formation of small amounts of **M1·(LiCl)$_2$·M1** (Scheme 6) is thermodynamically possible. Most probably, this complex is formed by dimerization of **D2** with **Li1** via a cubic intermediate, presumably **Li1·D2-cube(D)** at temperatures below −55 °C. Our NMR investigations show also that ^{i}Pr$_2$NMgCl·LiCl **2** does not produce SSIPs in detectable concentrations.[43] Further, the proposal that the impact of LiCl on the higher reactivity of *Turbo* bases rests on the deaggregation of RMgX oligomers to monomers has to be revised. Most reactions of RMgX reagents proceed in THF solution, and it is known for a long time that alkyl and aryl Grignard reagents are monomeric in THF solution.[8] Our results show that the same is true for Hauser base **1**. Moreover, the reason for the lower reactivity of LiCl-free Hauser bases should be reflected in the Schlenk-equilibrium. At low temperatures, the equilibrium in THF solution is mostly shifted to the side of homoleptic diamidomagnesium R$_2$Mg, where the amide ligands are highly sterically hindered in

Scheme 6. Determined Composition of *Turbo*-Hauser Base ^{i}Pr$_2$NMgCl·LiCl 2 in THF-d_8 Solution[a]

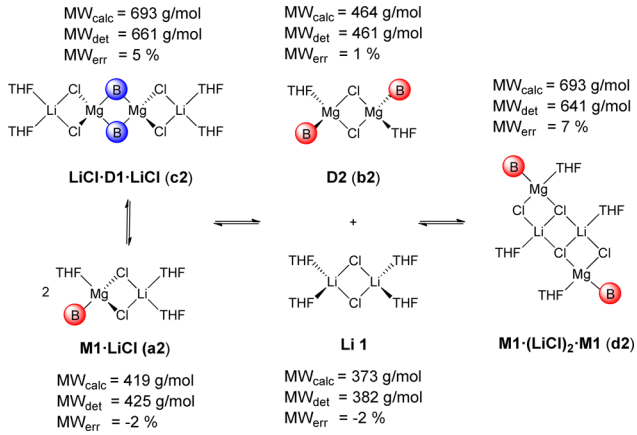

[a]At room temperature, the equilibrium is highly on the left side. At low temperature it moves significantly to the middle. The MWs were derived from ^{1}H and ^{7}Li DOSY-ECC-MW-determinations.[17] The accuracy of this method is in the range of MW$_{err}$ < ±9%.[35]

comparison with the heteroleptic RMgCl monomers and MgCl$_2$ cocoordinated species. These compounds that represent the most reactive species in a Hauser base solution are only present at low concentrations. This explains why it is necessary to use a large excess of Hauser bases (2–12-fold) to achieve high conversions in synthesis.[5d] The big advantage of LiCl is the ability to shift the Schlenk-equilibrium from the homoleptic to the heteroleptic side, especially at low temperatures. The high concentration of bimetallic complexes (like monomeric **M1·LiCl** (**a1**) as well as dimeric **LiCl·D1·LiCl** (**c2**), **D2** (**b2**), and **M1·(LiCl)$_2$·M1** (**d2**) should provide the most influence on the reactivity, chemoselectivity, and complex-induced proximity effects (CIPE)[52] of *Turbo*-Hauser bases. It is possible that this concept could also be applied to *Turbo*-Grignard reagents. Related studies are in progress.

CONCLUSION

Our investigation provides a deep insight into the solution structure of the Hauser base ^{i}Pr$_2$NMgCl **1** and its *Turbo* derivative ^{i}Pr$_2$NMgCl·LiCl **2**. We were able to show that their aggregation in THF-d_8 differs significantly and that the solution composition of the existing species is highly temperature dependent. Knowing the state of the equilibrium is of essential importance for every synthetic chemist, because Hauser bases as well as their *Turbo* analogues are used in synthesis at variable temperatures (−75 to 25 °C).[5d,53] The solution structure of **1** is best represented by the common Schlenk-equilibrium (eq 1) ^{i}Pr$_2$NMgCl (**M1**) ⇋ (^{i}Pr$_2$N)$_2$Mg (**M2**) + MgCl$_2$, with heteroleptic **M1** to be the main species at high temperatures and homoleptic **M2** at low temperatures (Scheme 7A). However, our work demonstrates that in Hauser base **1**, dimeric **D1** and **D2** are also present in the THF solution, although alkyl magnesium chlorides do not dimerize in that solvent. Therefore, the Hauser base **1** Schlenk-equilibrium has to be extended to dimeric amido bridged species **D1** as well as to MgCl$_2$ cocoordinated species **M1(μCl)$_3$MgCl$_2$** and **[^{i}Pr$_2$NMgCl]$_x$·[MgCl$_2$]$_y$·[THF]$_z$**, which exist only at low temperatures, where an excess of MgCl$_2$ is present. Our investigations also show that the addition of LiCl to **1** has an enormous impact on the Schlenk-equilibrium. The main

DOI: 10.1021/jacs.6b00345
J. Am. Chem. Soc. 2016, 138, 4796–4806

Scheme 7. Main Species of Hauser Base $^{i}Pr_2NMgCl$ 1 and *Turbo*-Hauser base $^{i}Pr_2NMgCl{\cdot}LiCl$ 2 in THF-d_8 Solution

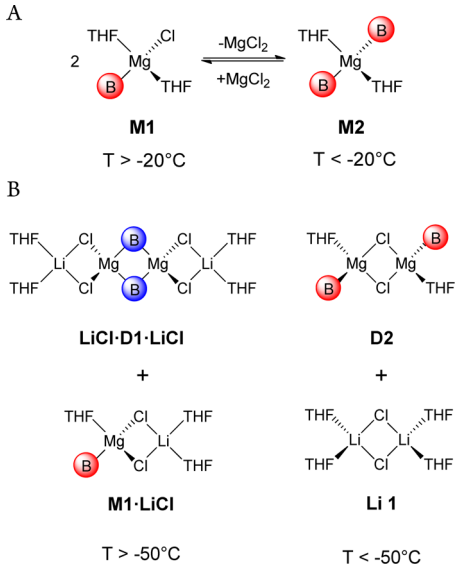

advantage of LiCl is the ability to shift the Schlenk-equilibrium from the homoleptic to the heteroleptic side. At room temperature, monomeric **M1·LiCl** and dimeric **LiCl·D1·LiCl** are the main species in solution of **2** (Scheme 7B), while the latter is the most populated species at high concentration (0.5–0.6 M). Lowering the temperature below −50 °C results in the formation of an equilibrium of **D2** and the LiCl-dimer **Li1** that stabilizes the heteroleptic dimer **D2** and inhibits the formation of homoleptic $(^{i}Pr_2N)_2Mg$ (**M2**) and $MgCl_2$.

EXPERIMENTAL SECTION

X-ray Analysis. Single crystals were mounted due to their sensitivity and reactivity in inert perfluorinated oil.[20] The X-ray data set of $[\mathbf{1}{\cdot}THF]_2$ was collected at 100(2) K on a Bruker Smart Apex II Quazar diffractometer with an INCOATEC micro source[54] equipped with mirror-monochromated Mo K_α radiation (λ = 0.71073 Å). The structure was solved by direct methods with SHELXT[55] and refined by full-matrix least-squares on F^2 for all data with SHELXL.[56] Non-hydrogen atoms were refined with anisotropic displacement parameters. All hydrogen atoms were placed in calculated positions and refined using a riding model. The structure is severely disordered and refined with distances restraints and restraints for the anisotropic displacement parameters.[57]

Crystal Data for $[\mathbf{1}{\cdot}THF]_2$. $C_{20}H_{44}Cl_2Mg_2N_2O_2$, M = 464.09 g/mol, monoclinic, space group $P2_1/n$, a = 9.766(2), b = 9.648(2), c = 14.138(3) Å, β = 110.00(2)°, Z = 2, V = 1251.8(4) Å^3, μ(Mo K_α) = 0.327 mm^{-1}, 33 818 reflections collected, 2666 independent reflections (R_{int} = 3.91%), θ_{max} = 26.75°, 230 parameters refined, 686 restraints used, $R_1[I > 2\sigma(I)]$ = 3.00%, wR_2(all data) = 7.96%, GOF = 1.067, largest diff. peak and hole 0.285 and −0.167 e Å^{-3}. Crystallographic data for compound $[\mathbf{1}{\cdot}THF]_2$ have been deposited at the Cambridge Crystallographic Data Centre CCDC 1423230.

Preparation of Crystalline $[\mathbf{1}{\cdot}THF]_2$. $^{i}PrMgCl$ (62.10 mmol, 31.05 mL, 2 M in THF, 1.0 equiv) was added dropwise to bulk diisopropylamine $^{i}Pr_2NH$ (68.31 mmol, 9.60 mL, 1.1 equiv) at room temperature. Stirring overnight and removal of the solvent in vacuo yielded an off-white powder (11.68 g, 96%, considering the loss of one molecule of THF of $[\mathbf{1}{\cdot}THF]_2$). To receive crystalline product, a saturated THF solution (24 mL) of $[\mathbf{1}{\cdot}THF]_2$ was prepared at room temperature. After reducing the solvent, addition of 5 mL of toluene, and storage at −6 °C, $[\mathbf{1}{\cdot}THF]_2$ was isolated as colorless crystals.

Preparation of Crystalline $[\mathbf{2}{\cdot}THF]_2$. Following the procedure suggested by García-Álvarez and Mulvey et al.,[14] we synthesized the *Turbo*-Hauser base $[\mathbf{2}{\cdot}THF]_2$ by reaction of donor-base-free LDA[18] (0.43 g, 4.00 mmol, 1.0 equiv) with a suspension of $MgCl_2$ (0.38 g, 4.00 mmol, 1.0 equiv) in THF and stirred the mixture overnight at room temperature. Removing the solvent in vacuo and recrystallization (2×) in a 1:1 mixture of THF/hexane at −45 °C afforded $[\mathbf{2}{\cdot}THF]_2$ as colorless crystals.

DOSY Measurements. Dry THF-d_8 stored over 4 Å molecular sieves under argon was used. The NMR samples were prepared by dissolving crystals of $[\mathbf{1}{\cdot}THF]_2$ or $[\mathbf{2}{\cdot}THF]_2$ (each 0.10 M) and the DOSY reference 1-phenylnaphthalene (PhN, 0.02 M) under argon atmosphere in THF-d_8. The diffusion coefficients of the amide species were normalized to the fixed diffusion value of the internal reference PhN (log $D_{ref,fix}$(PhN) = −8.8812; for more information, see Supporting Information section IX).[17] NMR experiments were recorded on two devices: (1) Bruker Avance 400 spectrometer equipped with a observe broadband probe with z-axis gradient coil with maximum gradient strength of 57 G/cm and (2) Bruker Ascend 400 spectrometer equipped with an inverse broadband probe with z-axis gradient coil with maximum gradient strength of 51 G/cm. All spectra were acquired using 5 mm NMR tubes, which were not spun during the measurements. All DOSY experiments were performed using a double stimulated echo sequence with bipolar gradient pulses and three spoil gradients with convection compensation (dstebpgp3s).[58] The duration of the magnetic field pulse gradients was adjusted for every temperature in a range of $\delta/2$ = 400–3500 μs. The diffusion time was Δ = 0.1 s. The delay for gradient recovery was 0.2 ms, and the eddy current delay was 5 ms. In each PFG NMR experiment, a series of 16 spectra on 32 K data points were collected. The pulse gradients were incremented from 2% to 98% of the maximum gradient strength in a linear ramp. After Fourier transformation and baseline correction, the diffusion dimension was processed with the Topspin 3.1 software. Diffusion coefficients, processed with a line broadening of 2 Hz, were calculated by Gaussian fits with the T1/T2 software of Topspin.

Computational Details. All structures included in this study were optimized at the B3LYP-D3/def2-SVP level of theory[29] (the dispersion corrections were computed with Becke-Johnson type damping).[59] The electronic energies were recomputed with the def2-TZVP basis set.[29b] Solvation effects were included through the use of the COSMO continuum model[60] both in the energy and in the optimization runs. All stationary points were confirmed to be true minima on the potential energy surface through harmonic vibrational calculations. All thermodynamic correction terms were derived from the latter. To deal with the large errors associated with low-energy vibrational modes (particularly in large complexes), we applied the quasi-rigid rotor harmonic oscillator formula proposed by Grimme,[61] with a cutoff parameter of 100 cm^{-1}. Furthermore, corrections were included to the entropy to account for the overestimation of translational freedom in solution. The latter was included taking a cell model for the change in translational degrees of freedom.[50] All reported energy values, unless otherwise noted, correspond to Gibbs free energies. All calculations were carried out with the Orca 3.0.3 program package.[62]

ASSOCIATED CONTENT

Supporting Information

The Supporting Information is available free of charge on the ACS Publications website at DOI: 10.1021/jacs.6b00345.

Detailed information about the NMR measurements, the DOSY-ECC-MW-determinations, and theoretical calculations (PDF)

X-ray data for compound $[\mathbf{1}{\cdot}THF]_2$ (CIF)

AUTHOR INFORMATION

Corresponding Author

*dstalke@chemie.uni-goettingen.de

DOI: 10.1021/jacs.6b00345
J. Am. Chem. Soc. 2016, 138, 4796–4806

Notes

The authors declare no competing financial interest.

■ ACKNOWLEDGMENTS

We are grateful to the DNRF funded Centre of Materials Crystallography (DNRF93), and we appreciate chemical donations from Rockwood Lithium. We are grateful to the undergraduate materials science students Annegret Lehmberg, Benjamin Neding, Hendrik Alexander Schwenson, and Sinja Pagel for preparing Hauser bases.

■ REFERENCES

(1) (a) Rathman, T. L.; Schwindeman, J. A. *Org. Process Res. Dev.* **2014**, *18*, 1192−1210. (b) Mulvey, R. E.; Robertson, S. D. *Angew. Chem.* **2013**, *125*, 11682−11700; *Angew. Chem., Int. Ed.* **2013**, *52*, 11470−11487.

(2) Hauser, C. R.; Walker, H. G. *J. Am. Chem. Soc.* **1947**, *69*, 295−297.

(3) Eaton, P. E.; Lee, C. H.; Xiong, Y. *J. Am. Chem. Soc.* **1989**, *111*, 8016−8018.

(4) (a) Shilai, M.; Kondo, Y.; Sakamoto, T. *J. Chem. Soc. Perkin Trans. 1* **2001**, 442−444. (b) Kondo, Y.; Yoshida, A.; Sakamoto, T. *J. Chem. Soc., Perkin Trans. 1* **1996**, 2331−2332.

(5) (a) Melzig, L.; Rauhut, C. B.; Knochel, P. *Chem. Commun.* **2009**, 3536−3538. (b) Rohbogner, C. J.; Wunderlich, S. H.; Clososki, G. C.; Knochel, P. *Eur. J. Org. Chem.* **2009**, *2009*, 1781−1795. (c) Clososki, G. C.; Rohbogner, C. J.; Knochel, P. *Angew. Chem.* **2009**, *119*, 7825−7828; *Angew. Chem., Int. Ed.* **2007**, *46*, 7681−7684. (d) Krasovskiy, A.; Krasovskaya, V.; Knochel, P. *Angew. Chem.* **2006**, *118*, 3024−3027; *Angew. Chem., Int. Ed.* **2006**, *45*, 2958−2961.

(6) Allan, J. F.; Clegg, W.; Henderson, K. W.; Horsburgh, L.; Kennedy, A. R. *J. Organomet. Chem.* **1998**, *559*, 173−179.

(7) Schlenk, W.; Schlenk, W. *Ber. Dtsch. Chem. Ges. B* **1929**, *62*, 920−924.

(8) Walker, F. W.; Ashby, E. C. *J. Am. Chem. Soc.* **1969**, *91*, 3845−3850.

(9) (a) Seven, Ö.; Bolte, M.; Lerner, H.-W. *Acta Crystallogr., Sect. E: Struct. Rep. Online* **2013**, *69*, m424−m424. (b) Nesbit, M. A.; Gray, D. L.; Girolami, G. S. *Acta Crystallogr., Sect. E: Struct. Rep. Online* **2012**, *68*, m942. (c) Ren, W.; Zi, G.; Fang, D.-C.; Walter, M. D. *Chem. - Eur. J.* **2011**, *17*, 12669−12682. (d) Avent, A. G.; Caro, C. F.; Hitchcock, P. B.; Lappert, M. F.; Li, Z.; Wei, X.-H. *Dalton Trans.* **2004**, 1567−1577. (e) Spek, A. L.; Voorbergen, P.; Schat, G.; Blomberg, C.; Bickelhaupt, F. *J. Organomet. Chem.* **1974**, *77*, 147−151. (f) Guggenberger, L. J.; Rundle, R. E. *J. Am. Chem. Soc.* **1968**, *90*, 5375−5378.

(10) (a) Ashby, E. C.; Smith, M. B. *J. Am. Chem. Soc.* **1964**, *86*, 4363−4370. (b) Ashby, E. C.; Becker, W. E. *J. Am. Chem. Soc.* **1963**, *85*, 118−119.

(11) Smith, M. B.; Becker, W. E. *Tetrahedron* **1967**, *23*, 4215−4227.

(12) (a) Ashby, E. C.; Nackashi, J.; Parris, G. E. *J. Am. Chem. Soc.* **1975**, *97*, 3162−3171. (b) Ashby, E. C.; Parris, G. E. *J. Am. Chem. Soc.* **1971**, *93*, 1206−1213. (c) Ashby, E. C.; Yu, S. *J. Organomet. Chem.* **1971**, *29*, 339−348.

(13) Seyferth, D. *Organometallics* **2009**, *28*, 1598−1605.

(14) Armstrong, D. R.; García-Álvarez, P.; Kennedy, A. R.; Mulvey, R. E.; Parkinson, J. A. *Angew. Chem.* **2010**, *122*, 3253−3256; *Angew. Chem., Int. Ed.* **2010**, *49*, 3185−3188.

(15) Because of signal overlap problems, the authors had to use internal references with inappropriate geometries. This setup produced a molecular weight (MW) determination with an error bar of approximately ±30%.

(16) Li, D.; Keresztes, I.; Hopson, R.; Williard, P. G. *Acc. Chem. Res.* **2009**, *42*, 270−280.

(17) Neufeld, R.; Stalke, D. *Chem. Sci.* **2015**, *6*, 3354−3364.

(18) Neufeld, R.; John, M.; Stalke, D. *Angew. Chem.* **2015**, *127*, 7100−7104; *Angew. Chem., Int. Ed.* **2015**, *54*, 6994−6998.

(19) (a) Niklas, T.; Stalke, D.; John, M. *Chem. Commun.* **2015**, *51*, 1275−1277. (b) Pöppler, A.-C.; Granitzka, M.; Herbst-Irmer, R.; Chen, Y.-S.; Iversen, B. B.; John, M.; Mata, R. A.; Stalke, D. *Angew. Chem.* **2014**, *126*, 13498−13503; *Angew. Chem., Int. Ed.* **2014**, *53*, 13282−13287. (c) Pöppler, A.-C.; Frischkorn, S.; Stalke, D.; John, M. *ChemPhysChem* **2013**, *14*, 3103−3107. (d) Pöppler, A.-C.; Meinholz, M. M.; Faßhuber, H.; Lange, A.; John, M.; Stalke, D. *Organometallics* **2012**, *31*, 42−45. (e) Granitzka, M.; Pöppler, A.-C.; Schwarze, E. K.; Stern, D.; Schulz, T.; John, M.; Herbst-Irmer, R.; Pandey, S. K.; Stalke, D. *J. Am. Chem. Soc.* **2012**, *134*, 1344−1351. (f) Pöppler, A.-C.; Keil, H.; Stalke, D.; John, M. *Angew. Chem.* **2012**, *124*, 7963−7967; *Angew. Chem., Int. Ed.* **2012**, *51*, 7843−7846.

(20) (a) Stalke, D. *Chem. Soc. Rev.* **1998**, *27*, 171−178. (b) Kottke, T.; Stalke, D. *J. Appl. Crystallogr.* **1993**, *26*, 615−619.

(21) García-Álvarez, P.; Graham, D. V.; Hevia, E.; Kennedy, A. R.; Klett, J.; Mulvey, R. E.; O'Hara, C. T.; Weatherstone, S. *Angew. Chem.* **2008**, *120*, 8199−8201; *Angew. Chem., Int. Ed.* **2008**, *47*, 8079−8081.

(22) (a) Yang, K.-C.; Chang, C.-C.; Huang, J.-Y.; Lin, C.-C.; Lee, G.-H.; Wang, Y.; Chiang, M. Y. *J. Organomet. Chem.* **2002**, *648*, 176−187. (b) Bartlett, R. A.; Olmstead, M. M.; Power, P. P. *Inorg. Chem.* **1994**, *33*, 4800−4803.

(23) Kennedy, A. R.; Mulvey, R. E.; Robertson, S. D. *Dalton Trans.* **2010**, *39*, 9091−9099.

(24) Cambridge Structural Database CSD, version 5.36 (Updated Nov 2014), chelating amido ligands have been excluded.

(25) Batsanov, A. S.; Bolton, P. D.; Copley, R. C. B.; Davidson, M. G.; Howard, J. A. K.; Lustig, C.; Price, R. D. *J. Organomet. Chem.* **1998**, *550*, 445−448.

(26) Deuterated species diffuse like their protonated counterparts. This is why we used MW_{calc}(THF) = 72.11 g/mol in the calculation of all THF coordinated species. For more information, see ref 17.

(27) All MW_{det} values are dispayed for each species as an average value, derived from DOSY-ECC-MW measurements at different temperatures; see Tables S3 and S6.

(28) Rappoport, Z.; Marek, I. *The Chemistry of Organomagnesium Compounds, Part I*; John Wiley & Sons Ltd: West Sussex, England, 2008.

(29) (a) Grimme, S.; Antony, J.; Ehrlich, S.; Krieg, H. *J. Chem. Phys.* **2010**, *132*, 154104. (b) Weigend, F.; Ahlrichs, R. *Phys. Chem. Chem. Phys.* **2005**, *7*, 3297−3305. (c) Becke, A. D. *J. Chem. Phys.* **1993**, *98*, 5648−5652. (d) Becke, A. D. *Phys. Rev. A: At., Mol., Opt. Phys.* **1988**, *38*, 3098−3100. (e) Lee, C.; Yang, W.; Parr, R. G. *Phys. Rev. B: Condens. Matter Mater. Phys.* **1988**, *37*, 785−789.

(30) (a) Stern, D.; Granitzka, M.; Schulz, T.; Stalke, D. *Z. Naturforsch., B: J. Chem. Sci.* **2010**, *65b*, 719−724. (b) Tammiku-Taul, J.; Burk, P.; Tuulmets, A. *J. Phys. Chem. A* **2004**, *108*, 133−139.

(31) Sakamoto, S.; Imamoto, T.; Yamaguchi, K. *Org. Lett.* **2001**, *3*, 1793−1795.

(32) Unfortunately, below −80 °C, the signal was too low in intensity for an accurate ECC-MW-determination.

(33) Blasberg, F.; Bolte, M.; Wagner, M.; Lerner, H.-W. *Organometallics* **2012**, *31*, 1001−1005.

(34) Species **$MgCl_2$·D1(D2)·$MgCl_2$** have a highly increased molar van der Waals density (MD_w). This is why a density correction has been done on the MW_{det} value of species **$MgCl_2$·D1(D2)·$MgCl_2$**; see Supporting Information section XXXIII.

(35) The deviation is calculated by $MW_{err} = [1 - MW_{det}/MW_{calc}]\cdot 100\%$, where MW_{det} is the experimentally determined and MW_{calc} is the calculated molecular weight.

(36) (a) Krasovskiy, A.; Straub, B. F.; Knochel, P. *Angew. Chem.* **2006**, *118*, 165−169; *Angew. Chem., Int. Ed.* **2006**, *45*, 159−162. (b) Krasovskiy, A.; Knochel, P. *Angew. Chem.* **2004**, *116*, 3396−3399; *Angew. Chem., Int. Ed.* **2004**, *43*, 3333−3336.

(37) (a) Yakimansky, A. V.; Müller, A. H. E.; Van Beylen, M. *Macromolecules* **2000**, *33*, 5686−5692. (b) Ming Keong, W.; Popov, A. I. *J. Inorg. Nucl. Chem.* **1972**, *34*, 3615−3622. (c) Bauer, S. H.; Ino, T.; Porter, R. F. *J. Chem. Phys.* **1960**, *33*, 685−691.

(38) (a) Elschenbroich, C.; Hensel, F.; Hopf, H. In *Organometallchemie*; Teubner, B. G., Ed.; Verlag: Wiesbaden, 2008; Vol. 6. (b) Gornitzka, H.; Stalke, D. *Angew. Chem.* **1994**, *106*, 695−698; *Angew. Chem., Int. Ed. Engl.* **1994**, *33*, 693−695. (c) In ref 14 the

DOI: 10.1021/jacs.6b00345
J. Am. Chem. Soc. 2016, 138, 4796−4806

authors already showed in accord with our findings that the ^{7}Li chemical shift of **2** displays a positive δ value even in a wide concentration range (higher than 0.21 ppm).
(39) The ^{7}Li NMR chemical shifts are referenced externally to LiCl in D_2O at 0.00 ppm.
(40) This behavior could be also attributed to a fast exchange of **LiCl·D1·LiCl** with its lithium free counterpart **D2** or to a dissociation into monomeric **M1·LiCl**. Both equilibria would produce a smaller effective MW.
(41) The ^{1}H NMR spectrum of **2** shows at −100 °C one broad signal. However, it was possible to distinguish **b2** and **d2** in the DOSY NMR experiment due to the high difference in the MW and diffusion coefficient, respectively; see Figure S31.
(42) To prove the structure of LiCl in THF, we measured anhydrous LiCl in THF-d_8. Our ^{7}Li ECC-MW-determination confirms the dimeric structure (**Li1**) of LiCl in THF solution (from 25 to −75°C, on av: MW_{calc} = 373 g/mol, MW_{det} = 381 g/mol, MW_{err} = −2%; see Table S7). That result stays in very good agreement with previous work from Reich et al. who categorized LiCl as a sturdy dimer (**Li1**) according to HMPA titrations: Reich, H. J.; Borst, J. P.; Dykstra, R. R.; Green, P. D. *J. Am. Chem. Soc.* **1993**, *115*, 8728−8741. On the other hand, we could not confirm the SSIP $[Li(thf)_4]^+Cl^-$ published by: Fernández, I.; Martínez-Viviente, E.; Breher, F.; Pregosin, P. S. *Chem. - Eur. J.* **2005**, *11*, 1495−1506.
(43) Additionally, a detectable formation of the SSIP $[Li(thf)_4]^+$ **Li2** can be excluded (MW_{calc} = 295 g/mol, MW_{det} = 382 g/mol, MW_{err} = −29%).
(44) Based on statistics from the Cambridge Structural Database CSD, version 5.36 (updated Nov. 2014). Allen, F. H. *Acta Crystallogr., Sect. B: Struct. Sci.* **2002**, *58*, 380−388.
(45) (a) Vollet, J.; Hartig, J. R.; Baranowska, K.; Schnöckel, H. *Organometallics* **2006**, *25*, 2101−2103. (b) Casellato, U.; Ossola, F. *Organometallics* **1994**, *13*, 4105−4108.
(46) Jiménez-Halla, J. O. C.; Bickelhaupt, F. M.; Solà, M. *J. Organomet. Chem.* **2011**, *696*, 4104−4111.
(47) (a) Brym, M.; Jones, C.; Junk, P. C.; Kloth, M. *Z. Anorg. Allg. Chem.* **2006**, *632*, 1402−1404. (b) Courtenay, S.; Wei, P.; Stephan, D. W. *Can. J. Chem.* **2003**, *81*, 1471−1476. (c) Neumann, F.; Hampel, F.; Schleyer, P. v. R. *Inorg. Chem.* **1995**, *34*, 6553−6555. (d) Hoffmann, D.; Dorigo, A.; Schleyer, P. v. R.; Reif, H.; Stalke, D.; Sheldrick, G. M.; Weiss, E.; Geissler, M. *Inorg. Chem.* **1995**, *34*, 262−269.
(48) (a) Gridley, B. M.; Blundell, T. J.; Moxey, G. J.; Lewis, W.; Blake, A. J.; Kays, D. L. *Chem. Commun.* **2013**, *49*, 9752−9754. (b) Sutton, A. D.; Ngyuen, T.; Fettinger, J. C.; Olmstead, M. M.; Long, G. J.; Power, P. P. *Inorg. Chem.* **2007**, *46*, 4809−4814. (c) Batsanov, A. S.; Davidson, M. G.; Howard, J. A. K.; Lamb, S.; Lustig, C.; Price, D. R. *Chem. Commun.* **1997**, 1211−1212. (d) Buttrus, N. H.; Eaborn, C.; El-Kheli, M. N. A.; Hitchcock, P. B.; Smith, J. D.; Sullivan, A. C.; Tavakkoli, K. *J. Chem. Soc., Dalton Trans.* **1988**, 381−391.
(49) Grignard reagents are also known to be very weak electrolytes, see: Seyferth, D. *Organometallics* **2009**, *28*, 1598−1605.
(50) Ardura, D.; López, R.; Sordo, T. L. *J. Phys. Chem. B* **2005**, *109*, 23618−23623.
(51) Once again with a correction to the translational entropy.
(52) Whisler, M. C.; MacNeil, S.; Snieckus, V.; Beak, P. *Angew. Chem.* **2004**, *116*, 2256−2276; *Angew. Chem., Int. Ed.* **2004**, *43*, 2206−2225.
(53) Li-Yuan Bao, R.; Zhao, R.; Shi, L. *Chem. Commun.* **2015**, *51*, 6884−6900.
(54) Schulz, T.; Meindl, K.; Leusser, D.; Stern, D.; Graf, J.; Michaelsen, C.; Ruf, M.; Sheldrick, G. M.; Stalke, D. *J. Appl. Crystallogr.* **2009**, *42*, 885−891.
(55) Sheldrick, G. M. *Acta Crystallogr., Sect. A: Found. Adv.* **2015**, *71*, 3−8.
(56) Sheldrick, G. M. *Acta Crystallogr., Sect. C: Struct. Chem.* **2015**, *71*, 3−8.
(57) (a) Thorn, A.; Dittrich, B.; Sheldrick, G. M. *Acta Crystallogr., Sect. A: Found. Adv.* **2012**, *68*, 448−451. (b) Krause, L.; Herbst-Irmer, R.; Sheldrick, G. M.; Stalke, D. *J. Appl. Crystallogr.* **2015**, *48*, 3−10. (c) Müller, P.; Herbst-Irmer, R.; Spek, A. L.; Schneider, T. R.; Sawaya, M. R. *Crystal Structure Refinement−A Crystallographer's Guide to SHELXL*; Oxford University Press: Oxford, England, 2006.
(58) (a) Jerschow, A.; Müller, N. *J. Magn. Reson.* **1997**, *125*, 372−375. (b) Jerschow, A.; Müller, N. *J. Magn. Reson., Ser. A* **1996**, *123*, 222−225.
(59) (a) Johnson, E. R.; Becke, A. D. *J. Chem. Phys.* **2006**, *124*, 174104. (b) Becke, A. D.; Johnson, E. R. *J. Chem. Phys.* **2005**, *123*, 154101. (c) Johnson, E. R.; Becke, A. D. *J. Chem. Phys.* **2005**, *123*, 024101.
(60) Klamt, A.; Schüürmann, G. *J. Chem. Soc., Perkin Trans. 2* **1993**, 799−805.
(61) Grimme, S. *Chem. - Eur. J.* **2012**, *18*, 9955−9964.
(62) Neese, F. *WIREs Comput. Mol. Sci.* **2012**, *2*, 73−78.

DOI: 10.1021/jacs.6b00345
J. Am. Chem. Soc. 2016, 138, 4796−4806